International Journal of Trend in Scientific Research and Development (IJTSRD)
Volume 3 Issue 5, August 2019 Available Online: www.ijtsrd.com e-ISSN: 2456 – 6470

Porosity and the Magnetic Properties of Aluminium Doped Nickel Ferrite

Sandar Oo[1], Ye Wint Tun[2], Shwe Zin Oo[3]

[1]Department of Physics, University of Computer Studies, Loikaw, Myanmar
[2]Department of Physics, Maubin University, Myanmar
[3]Department of Physics, University of Computer Studies, Hpa-An, Myanmar

How to cite this paper: Sandar Oo | Ye Wint Tun | Shwe Zin Oo "Porosity and the Magnetic Properties of Aluminium Doped Nickel Ferrite" Published in International Journal of Trend in Scientific Research and Development (ijtsrd), ISSN: 2456-6470, Volume-3 | Issue-5, August 2019, pp.79-86, **https://doi.org/10.31142/ijtsrd25240**

IJTSRD25240

ABSTRACT

The nanocrystalline particles of Aluminium (Al) doped nickel (Ni) ferrites with general formula $NiAl_xFe_{2-x}O_4$ (x = 0.0, 0.2, 0.4, 0.6, 0.8 and 1.0) were synthesized by sol-gel auto-combustion technique. The formation of single phase cubic spinel was confirmed by X-ray diffraction analyses. Morphological features of the samples are studied by Scanning Electron Microscopy (SEM) to examine the particle size, shape and homogeneity of sample. The magnetic hysteresis graphs were obtained to understand their magnetic behaviours. The relative permeability (μ_r) of Al–Ni ferrite samples shows a decrease for all samples as Al content increases.

KEYWORDS: *Sol-gel; Crystallize Size; Porosity; Magnetic Properti*

1. INTRODUCTION

Ni spinel ferrites have high electrical resistivity, low dielectric and eddy current losses, which are a major factor for microwave devices [5]. The substituting of Al content into spinel ferrites matrix increases resistivity, lowers the dielectric losses, and thereby lowers the saturation magnetization [2,6]. Soft ferrites are the most widely used magnetic materials for low–cast, high–performance, and high- frequency applications. The applications of ferrites are remarkable due to their good electrical, magnetic and optical properties. Generally, the electrical resistivity of ferrites de-creases with the increase of temperature, which shows that ferrites have semiconductor behavior. In the present investigation we have employed sol-gel auto-combustion method to synthesize Al doped nickel ferrite nano-particles [3].

The sol-gel auto-combustion method is used to speed up the synthesis of complex materials. It is a simple process, which offers a significant saving in time and energy consumption over the traditional methods and requires less sintering temperature. This method is employed to obtain improved powder characteristics, better homogeneity and narrow particle size distribution, thereby influencing structural, electrical, and magnetic properties of spinel ferrites [1]. In the inverse spinel structure of $NiFe_2O_4$ the tetrahedral sites are occupied by ferric ions and octahedral sites by ferric and nickel ions. In this research, the effect of gradual replacement of Fe^{3+} ions by Al^{3+} ions in$NiAl_xFe_{2-x}O_4$ ferrites on the X–ray density, bulk density, porosity and magnetic properties.

The rest of this paper is arranged as follows. In Section 2, Experimental Instrumentation related literature to identify the key issues and summarize the experiences from varies studies in different countries about the topic. In Section 3, we describe the data, the procedures, the methodology and present related descriptive statistics. In Section 4, aluminium doped nickel ferrites associated with fatigue driving and/or the severity of fatigue-related crashes are reported. Conclusion of results is given in Section 5.

2. Experimental Instrumentation

2.1. X-Ray Diffraction (XRD) Measurement

Experimental conditions for XRD measurement were as follows:

HV	: 40 kV, 40 mA
Diffraction angle range	: 10˚-70˚
Scan speed	: 4˚/min
Detector	: NaI (Tl)
Target (Anode)	: Cu

The crystallite size of undoped and Al-doped $NiFe_2O_4$ present in the investigated solids has been based on X-ray diffraction line broadening and calculated by using Scherrer equation [10].

$$D = \frac{k\lambda}{B\cos\theta} \qquad \text{..... (1)}$$

where D is the average crystallite size of the phase under investigation, k is the Scherrer constant (0.9), λ is the wave length of X-ray beam used, B is the full-width at half maximum (FWHM) of diffraction and θ is the Bragg's angle [5].

Unit cell volume ($V=a^3$) was calculated and incorporated in the equation given below to calculate the X-ray densities (ρ_x) of all samples,

$$\rho_x = \frac{8M}{Na^3} \quad \text{..... (2)}$$

Where, M is molecular mass of the sample, '8' is the number of molecules is the cell, 'N' is the Avogadro's number and 'a' is the lattice parameters.

The bulk density of each composition was measured by using the equation is;

$$\rho_s = \frac{m}{\pi r^2 h} \quad \text{..... (3)}$$

Measurements were repeated on different powder of the same sample the average bulk density of each sample is determined.

The porosity P of the sample was calculated according to the relation:

$$P = 1 - \frac{\rho_s}{\rho_x} \quad \text{..... (4)}$$

Where, ρ_s is the bulk density of the sample and ρ_x is the X-ray density of the sample.

2.2. Scanning Electron Microscopy (SEM)

The device uses the electron beam to produce a magnified image of the sample. In the device, the electron gun produces a high- intensity electron beam, which passes through a series of electromagnetic lenses to be focused and scanned across the sample. The incident or primary electron beam causes secondary electrons to be emitted from the sample. Then, by using a variety of detectors, the image is reconstructed from the signals backscattered from the surface of the sample and magnified on the screen. The resolution of the SEM can approach a few nanometre (nm) and it can operate at magnifications that are easily adjusted from about 10X – 300,000X. SEM analyser of these ferrite samples revealed a strong influence of the processing and composition on the microstructure (grain size and morphology). The line intercept method is used to measure the grain size. Morphological features of Aluminium Doped Nickel-ferrite particles, $NiAl_xFe_{2-x}O_4$ (x = 0.0, 0.2, 0.4, 0.6, 0.8 and 1.0) have been investigated by SEM. In a SEM, these signals come out only from the primary beam impinging upon the sample, but from other interactions within the samples near the surface. The SEM is capable of producing high–resolution images of a sample surface in its primary use mode, secondary electron imaging. Due to the manner in which this image is created, SEM images have great depth of field yielding a characteristic three–dimensional appearance useful for understanding the surface structure of a sample. This great depth of field and the wide range of magnifications are the most familiar imaging mode for specimens in the SEM. Characteristic X-rays are emitted when the primary beam causes the ejection of inner shell electrons from the sample and are used to tell the elemental composition of the sample. The back scattered electrons emitted from the sample may be used alone to form an image or in conjunction with the characteristic X-rays as atomic number contrast clues to the elemental composition of the sample [14].

SEM measurement scans only about 1μm× 1μm area of the sample. In order to get the reliable data, a mathematical method must be developed. The grain size is estimated by using Line Intercept Method in this work. Two diagonals and two bisectors are drawn on the image. Then, the number of grains which is on the line is counted visually. When the length of the line is divided by the number of grains on that line, the average grain size is obtained. The procedure is repeated for four lines and the grand average is obtained. The Line Intercept Method is showed in Figure 1.

Figure 1 Line Intercept Method

2.3 FTIR Spectroscopic Measurement

Infrared spectroscopy is a chemical analytical technique which measures the infrared intensity versus wavelength (wave number) of light. Based upon the wave number, infrared light can be categorized as for infrared (4-400) cm^{-1}, mid infrared (400-4000) cm^{-1} and near infrared (4000-14000) cm^{-1}. The infrared absorption spectra of the ferrites were measured using Fourier Transform Infrared Spectrometer (FTIR – 8400 Shimadzu). The FTIR spectrum was measured where at least 80 scans and were collected at 16 cm^{-1} spectral resolution. In infrared spectroscopy, IR radiation is passed through a sample. Some the infrared radiation is observed by the sample some it is passed through (transmitted). Infrared spectroscopy is useful for several types of analysis. Fourier Transform Infrared Spectrometer (FTIR) spectroscopy [1] is based on the idea of the interference of radiation between two beams to yield an interferogram. The latter is a signal produced as a function of the change of path length between the two beams. The two domains of distance and frequency are interconvertible by the mathematical method of Fourier-transformation.

The radiation emerging from the source is passed through an interferometer to the sample before reaching a detector. Upon amplification of the signal, in which high-frequency contributions have been eliminated by a filter, the data are converted to digital form by an analog-to-digital converter and transferred to the computer for Fourier-transformation. In this work, ferrite samples were prepared prior for infrared excitation using the potassium bromide (KBr) pellet method on powdered samples. I referred to previous theory in my research work.

3. Methodology

3.1. Experimental Procedures

Aluminium substituted nickel-ferrite particles have been synthesized by sol-gel auto-combustion method. The Citric acid ($C_6H_8O_7.H_2O$), Nickel Nitrate ($Ni(NO_3)_2.6H_2O$), Ferric Nitrate ($Fe(NO_3)_3.9H_2O$), Aluminium Nitrate ($Al(NO_3)_3.9H_2O$) crystalline powders of $NiAlxFe_{2-x}O_4$ (x = 0.0, 0.2, 0.4, 0.6, 0.8 and 1.0) have been prepared by used as starting raw materials. The molar ratio of metal nitrates to citric acid has been taken as 1:3. The metal nitrates have been dissolved together in 100 ml of de-ionized water to get a clear solution. An aqueous solution of citric acid has been mixed with metal nitrates solution, then ammonia hydroxide solution has been slowly added to adjust the pH at 7. The mixed solution has been moved on to a hot plate with continuous stirring

between 90ºC and 100ºC. During evaporation, the solution became viscous and finally formed a very viscous brown gel. When finally, all remaining water was released from the mixture, the sticky mass began to bubble. After several minutes the gel automatically ignited and burnt with glowing flints. The decomposition reaction would not stop before the whole citrate complex was consumed. The auto ignition was completed within a minute, yielding the brown-colored ashes termed as a precursor. The as-prepared powder has been annealed at 700ºC for 3 hrs to get single phase spinel product and used for further characterization. Then, the powder has been pressed into pellets by hydraulic press at a pressure of 5 tons.

The phase formations of the pre-sintered samples have been characterized by XRD analysis. The final sintering has been performed at 900°C for 5hrs.The phase formations of the sintered samples have been characterized by XRD analysis and Fourier Transform Infrared Spectroscopy (FT-IR). By using from the XRD analysis have been calculated X-ray density, bulk density and porosity. After that, morphological feature of the sample is studied by Scanning Electron Microscope. And then all samples were polished and silver paste was applied on both sides of the polished pellet together with two thin copper wires. The variation of resistivity with temperature was measured by SUOER multimeter. The dielectric constants were measured in the frequency range of 1kHz to 10GHz. The electrical properties of samples have been measured using Fluke- 189 LCR meter in the low frequency range (1-1000) kHz and higher frequency range (1 kHz to 10GHz) at room temperature. And then, the pre-sintered powder was pressed into pellets of 1 inches diameter and approximately 3 mm thickness for measuring magnetic properties. The pallets were then finally sintered at 900°C for 5hrs in the furnace. Moreover, the magnetization and demagnetization of these samples were determined by PERMAGRAPH L technique. Figure 2 shows the flow chart of experimental procedure.

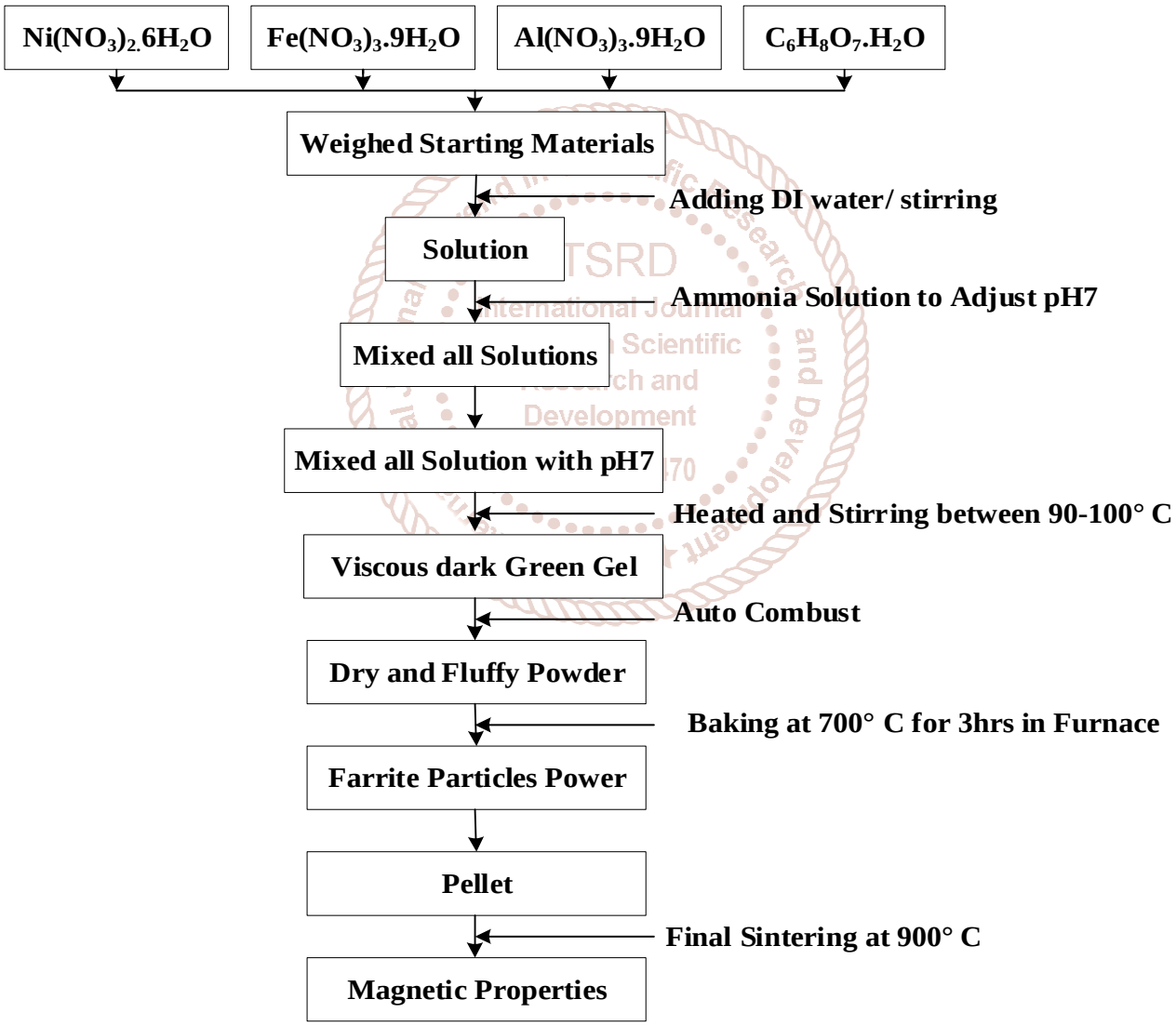

Figure 2 Flow chart of experimental procedure

4. Analytical Results and Discussion

Aluminium substituted Nickel-ferrite, $NiAl_xFe_{2-x}O_4$ (x = 0.0, 0.2, 0.4, 0.6, 0.8 and 1.0) have been synthesized by sol-gel auto combustion method. The structural characterization of the ferrites was employed by powder X-ray diffraction technique and FTIR spectroscopic measurement. The surfaces have been studied by performing Scanning Electron Microscope measurement. The main part of the recent paper has been important on the investigation of the electrical and magnetic properties of the Aluminium substituted Nickel-ferrite.

4.1. X-ray Diffraction Analysis

X-ray diffractograms of $NiAl_xFe_{2-x}O_4$ (x = 0.0, 0.2, 0.4, 0.6, 0.8 and 1.0) samples are shown in Figure 3 (a, b, c, d, e, f and g).

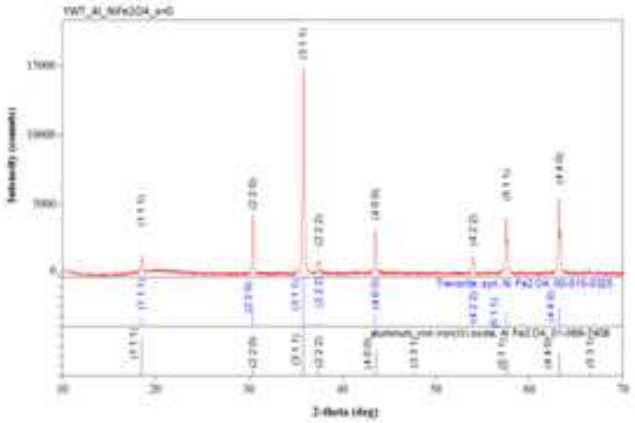

Figure 3(a) x = 0.0

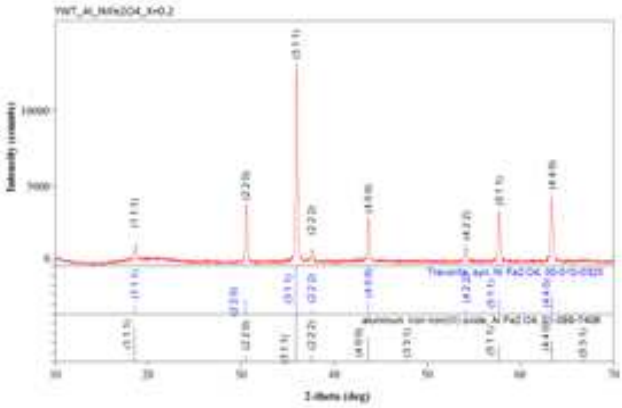

Figure 3(b) x = 0.2

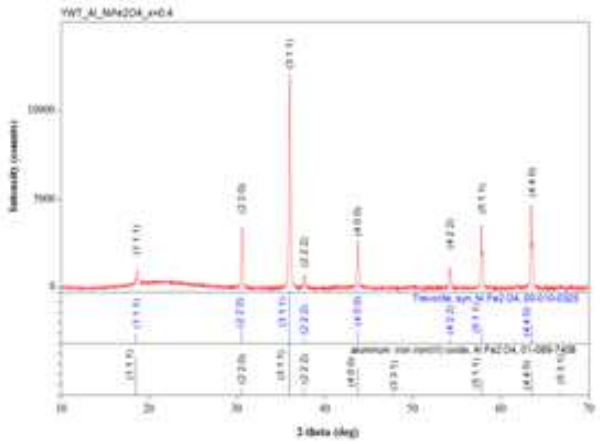

Figure 3(c) x = 0.4

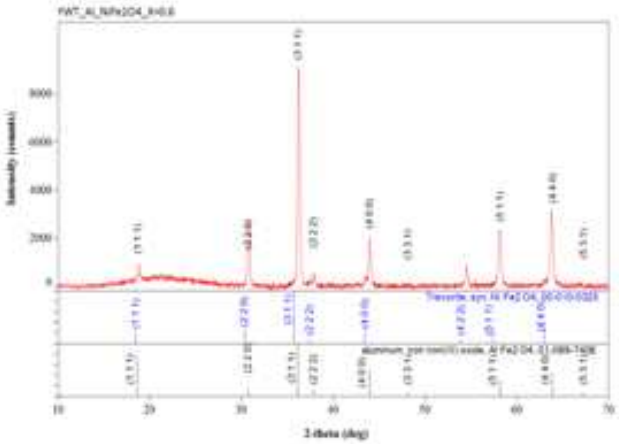

Figure 3(d) x = 0.6

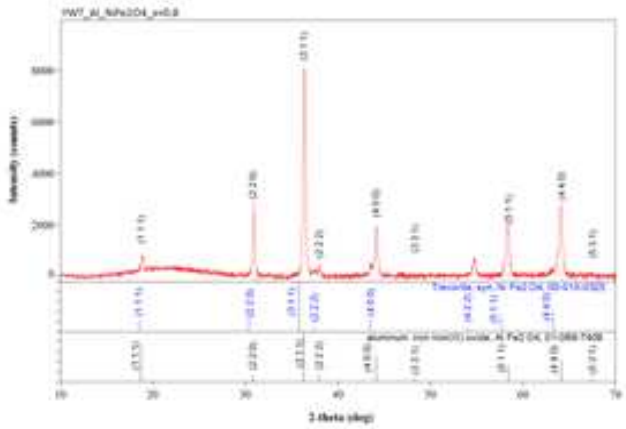

Figure 3(e) x = 0.8

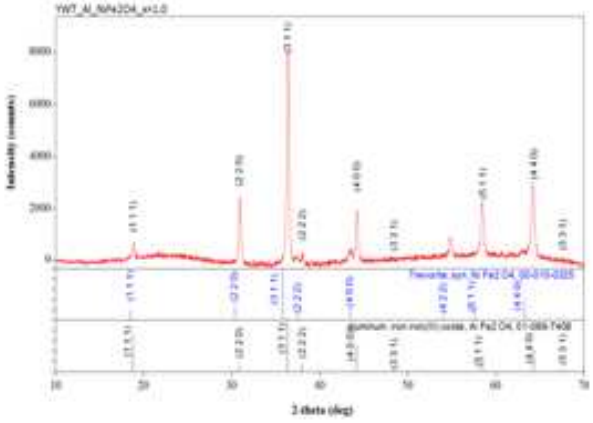

Figure 3(f) x = 1.0

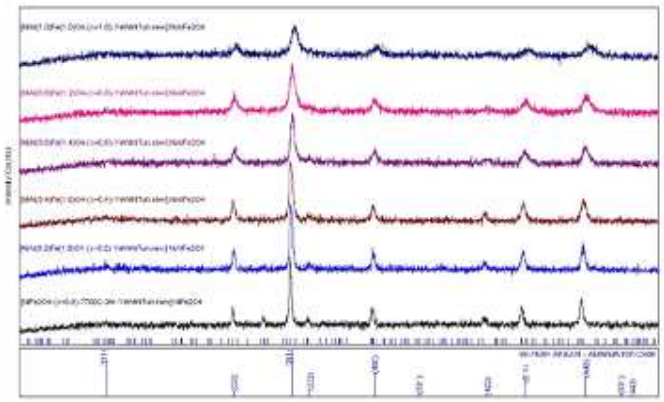

Figure 3 (g) XRD pattern of $NiAl_xFe_{2-x}O_4$ (x = 0.0, 0.2, 0.4, 0.6, 0.8, 1.0) after final sintering at 900° C

This XRD diffractograms display formation of well nano-crystalline undoped and Aluminium doped $NiFe_2O_4$ to be single cubic spinel phase with reflection planes of (2 2 0), (3 1 1), (4 0 0), (4 2 2), (5 1 1) and (4 4 0). The XRD patterns clearly indicate that the prepared samples contain cubic spinel structure only. The strongest reflection peak has resulted from the (3 1 1) plane that indicates the spinel phase.

An increase of the aluminium content resulted in a measurable decrease in the degree of crystallinity of spinel nickel ferrite phase with subsequent a decrease in the intensity of its diffraction peaks. Some diffraction planes such as (2 2 0) and (4 4 0) planes are more sensitive to the cations distribution on tetrahedral and octahedral sites, respectively.

The sizes of crystallites in the sample have been evaluated by using the FWHM of the most intense peak (220) (311) (400) (511) (440). The crystallite size was calculated from the XRD peak of the (220) (311) (400) (511) (440) plane using Scherrer's formula. The results are shown in Table 1.

Table 1 Lattice constant, Porosity and crystallize size of the $NiAl_xFe_{2-x}O_4$

Composition (x)	Lattice constant(a)	Crystallize size	X-ray density (gcm^{-3})	Bulk density	Porosity (%)
0.0	8.31	49.45	4.40	1.67	62.00
0.2	8.29	31.86	4.09	2.01	50.74
0.4	8.28	28.75	3.82	2.13	44.33
0.6	8.23	22.94	3.61	2.15	41.27
0.8	8.20	22.41	3.54	2.17	38.54
1.0	8.19	21.68	3.45	2.34	32.19

From Table1, the lattice constant, crystallize size and porosity progressively has decreased with the increase of Al^{3+} ion concentration. The variation of crystallite size, X-ray density, Bulk density and Porosity with chemical composition of Al content 'x' is shown in Figure 4.

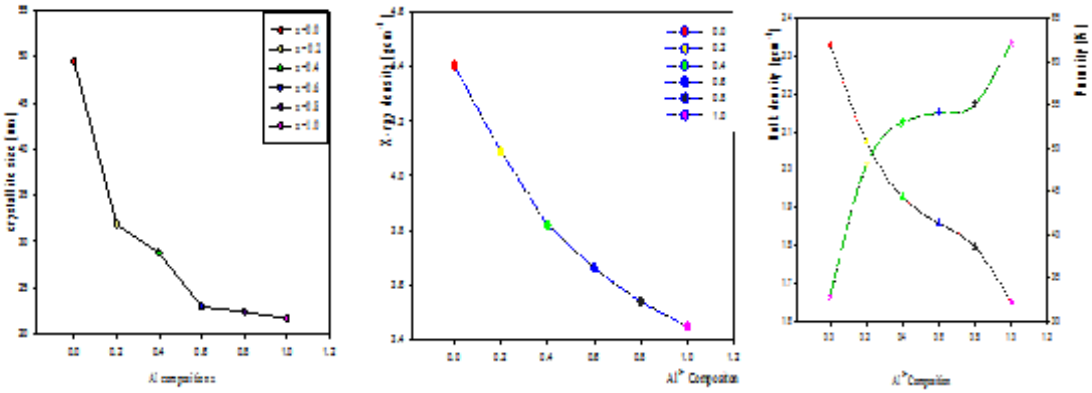

Figure 4 Variation of Crystallite size, X-ray density, Bulk density and Porosity with chemical composition x

4.2. Morphological Analysis

The microstructure of undoped and Al doped Ni ferrite have been revealed of $NiAl_xFe_{2-x}O_4$ (x = 0.0, 0.2, 0.4, 0.6, 0.8 and 1.0) samples are shown in Figure 5 (a, b, c, d, e and f). The SEM images are analyzed by using Line-Intercept Method to estimate the grain size. The calculated values of average grain size are presented in Table 2.

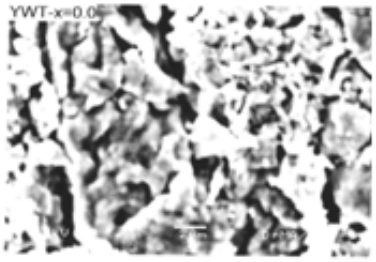

Figure 5(a) x=0.0

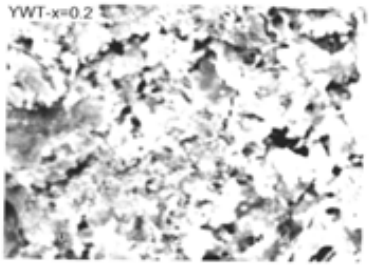

Figure 5(b) x=0.2

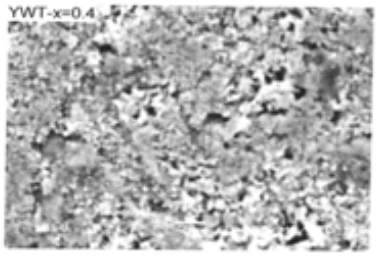

Figure 5(c) x=0.4

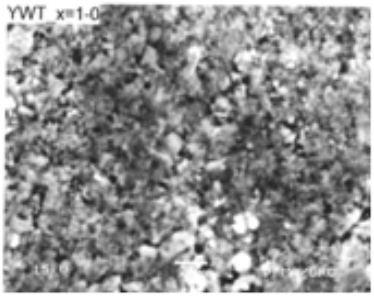

Figure 5(a) x=1.0

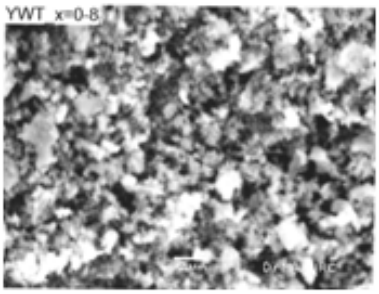

Figure 5(b) x=0.8

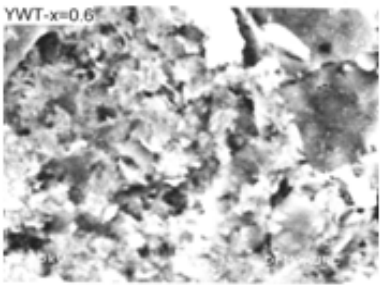

Figure 5(c) x=0.6

Table 2 the average grain size of $NiAl_xFe_{2-x}O_4$ pellets

Composition(x)	Grain Size (μm)
0.0	2.18
0.2	2.11
0.4	1.96
0.6	1.62
0.8	1.44
1.0	1.35

4.3. Hopping length

The distance between magnetic ions i.e. hopping length in tetrahedral site (L_A) and for the octahedral site (L_B) is given by the relations of lattice constants as follow.

$$L_A = \frac{a\sqrt{3}}{4} \quad (5)$$

$$L_B = \frac{a\sqrt{2}}{4} \quad (6)$$

Table 3 shows hopping length (L_A and L_B) of the $NiAl_xFe_{2-x}O_4$. The variation of hopping lengths with Al content 'x' is shown in Figure 6.

Table 3 Hopping length (L_A and L_B) of the $NiAl_xFe_{2-x}O_4$

Composition(x)	L_A	L_B
0.0	3.598	2.938
0.2	3.589	2.931
0.4	3.585	2.927
0.6	3.564	2.909
0.8	3.551	2.899
1.0	3.546	2.896

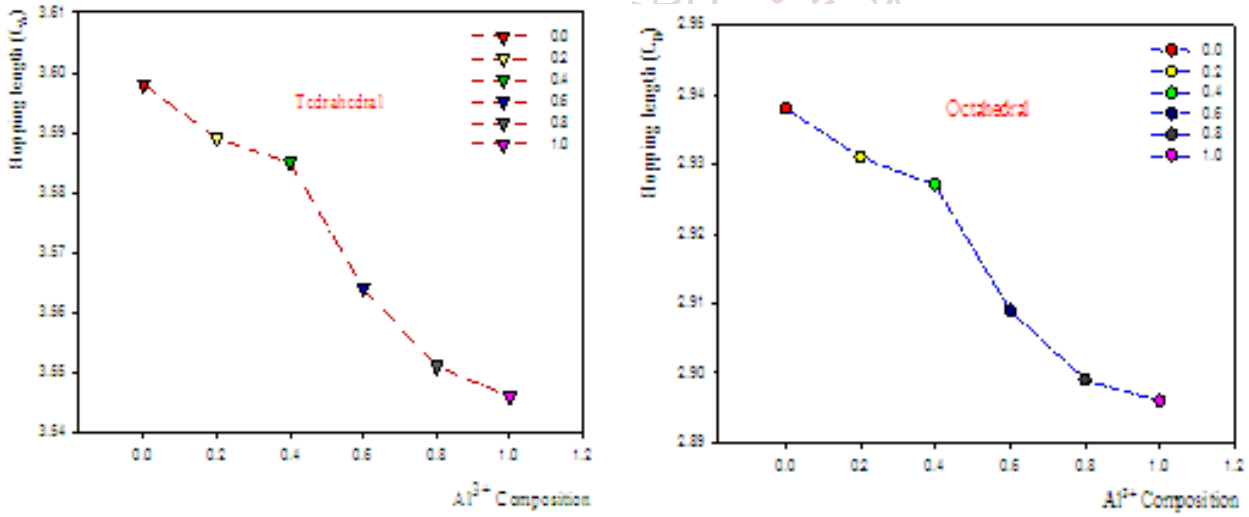

Figure 6 Variation of hopping length L_A and L_B with Al^{3+} concentration

It can be seen that hopping length (L_A and L_B) of Ni-Al ferrite decreases as increase in Al^{3+} content. It is attributed that the Hopping length has decreased due to the decrease in the lattice constant with increasing Al^{3+} content. Jump length for A-sites and B-sites were found to be decreased slightly with increasing Al^{3+} ion concentration. This shows that less energy is required for jumping of electrons between A-sites and B-sites as a result of which the conductivity increases.

4.4. Magnetic Properties

Magnetic properties were carried out by means of magnetization measurement to study the magnetic interaction between the ions. For measuring the field strength H, either integrated or separate field strength measuring coils has been used. As no space for the Hall probe is required, specimens of a thickness down to only 1 mm can be measured. Central component of the measuring instrument is an electromagnet that is used to magnetize and demagnetize the magnet specimen in order to cycle through the hysteresis loop. The magnetic field strength H and the magnetic polarization J are measured simultaneously with special measuring coils. Two integrators are required to process the output signals of the coils. The PERMAGRAPH®L uses a two-channel analogy precision flux meter integrator with 24 bits analog-to-digital converters. In an open magnetic circuit, the variation of J with H is usually measured and the coercivity is then denoted by H_{cJ}. The variation of the coercive force (H_{cj}) and remanence (B_r) have been observed by using B-H loop as shown in Figure 7 to 9.

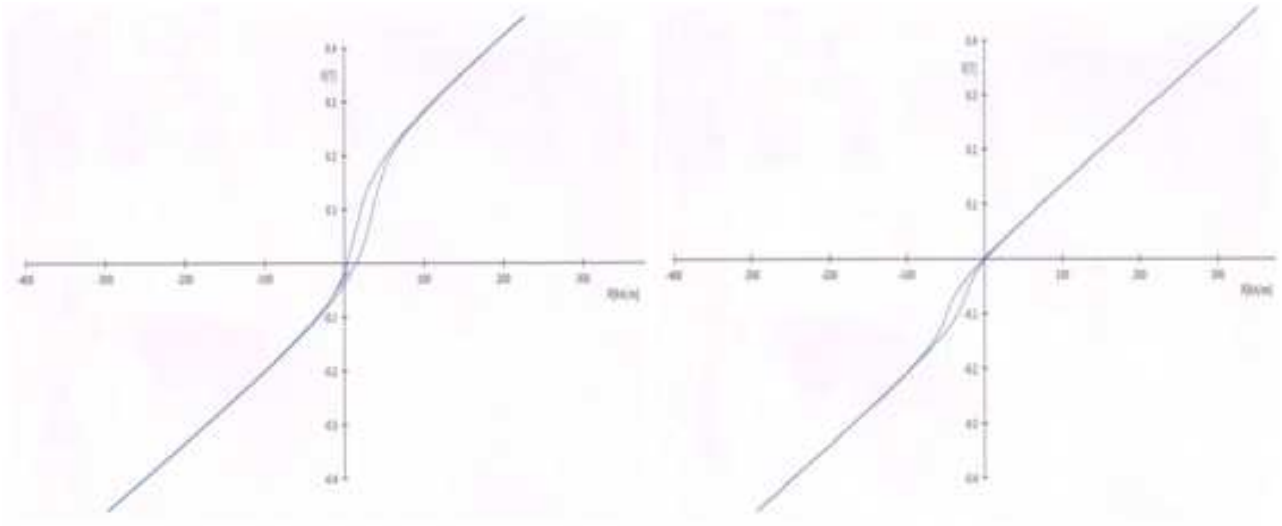

Figure 7 Hysteresis loop for $NiAl_xFe_{2-x}O_4$ (x =0.0 and x=0.2) sample

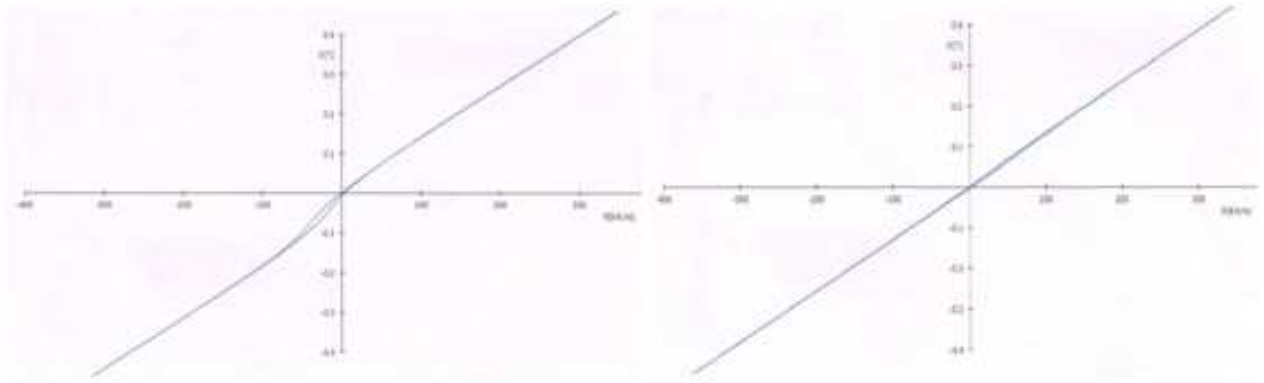

Figure 8 Hysteresis loop for $NiAl_xFe_{2-x}O_4$ (x = 0.4 and x=0.6) sample

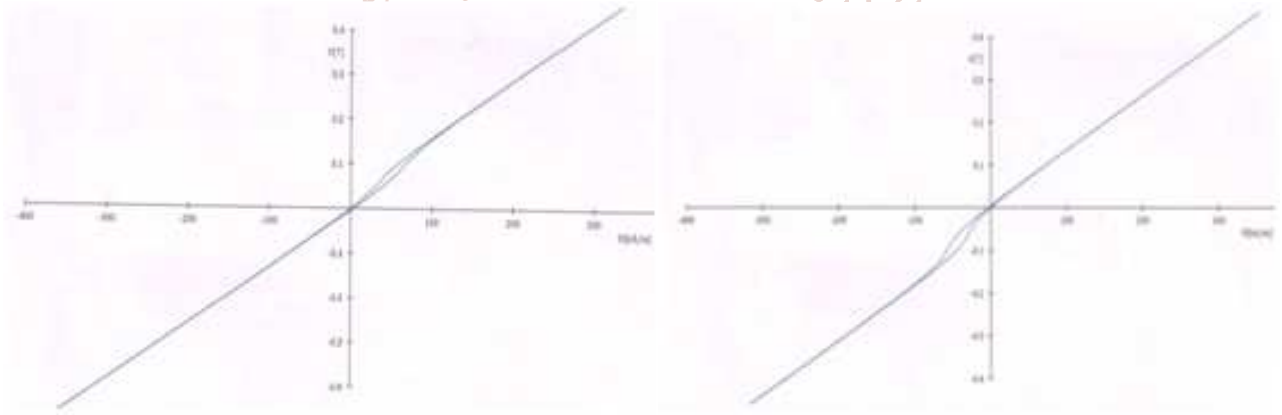

Figure 9 Hysteresis loop for $NiAl_xFe_{2-x}O_4$ (x = 0.8 and 1.0) sample

The permeability (μ) is defined as the ratio between the magnetic field B and H which is given by

$B = \mu H$ (7)

$\mu = \mu_r \mu_0$ (8)

where, μ_0 is the permeability of free space. From the magnetization graph, the Coercivity of J(H) curve, H_{cj} (intrinsic coercivity), remanence (B_r or J_r), Maximum energy product $(BH)_{max}$ and remanence permability (μ_{rec}) are estimated and are listed in Table4.

Table 4 the values of magnetic parameters from hysteresis loops

Composition (x)	B_r	H_{cj}	μ_r	(BH)max
0.0	0.013500	6.01	1.77	0.06500
0.2	0.002250	5.95	1.26	0.00062
0.4	0.001519	5.86	1.19	0.00020
0.6	0.001510	21.40	1.00	0.00027
0.8	0.000580	5.68	1.04	0.00005
1.0	0.000469	25.30	1.10	0.0033

Oxides that can easily lose magnetism are known as soft ferrite, whereas those that maintain it better are hard ferrites. The coercivity $H_c > 200$ is a hard ferrite, $H_c < 20$ is a soft ferrite and $20 < Hc < 200$ is semi-hard ferrite. Based on this background knowledge, the Al–Ni spinel ferrite may be considered as a soft ferrite material. However, $NiAl_xFe_{2-x}O_4$ (x=0.6 and x= 1.0) has shown semi-hard ferrite behavior. It is found that μ_{rec} decrease with increasing of Al^{3+} compositions as shown in Figure 10.

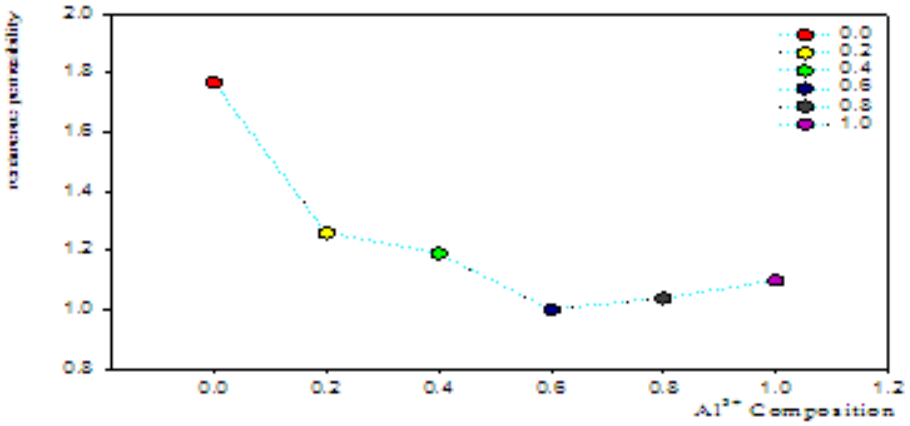

Figure 10 Variation of remanence permeability with Al^{3+}composition x

The remanence permeability μ_{rec} decreases with increasing of Al^{3+} compositions. It has been confirmed that the magnetic properties can be tuned by varying the amount of Al substitution.

5. Conclusion

This work studies on Aluminium (Al) doped into Nickel-ferrite with different Al ratio by sol-gel auto combustion method involving final sintering at 900ºC. The porosity decreased progressively with addition of aluminums nickel ferrite. It is observed that the distance between the magnetic ions decreases with the increase of the Al content due to the smaller ionic radius of Al^{+3} (53A°) compared to that of Fe^{+3} (64 A°) providing better electrical conduction. The remanence permeability μ_{rec} decrease with increasing of Al^{3+} compositions, so the Al–Ni spinel ferrite may be considered as a soft ferrite material. However, $NiAl_xFe_{2-x}O_4$ (x=0.6 and x= 1.0) has shown semi-hard ferrite behavior. Therefore, it is concluded that the magnetic properties can be tuned by varying the amount of Al substation.

References

[1] Auzans, E., Zins, D., Blums, E., &Massart, R. (1999). Synthesis and Properties of Ferrite.*Journal of Materials Science*, 34(6), 1253-1260.

[2] Bhosale A.G. and Chougule B.K., (2006), X-ray, infraredand magnetic studies of. Al-substituted Niferrites, *Materials Chemistry and Physics*, 97(s2–3), 273–276.

[3] Ghasemi, A., Ekhlasi, S. and Mousavinia, M. (2014). Structural andMagnetic Properties of Nickel Ferrite Synthesized by Using thesol-gel Auto-CombustionMethod.*Journal of Magnetism and Magnetic Materials*, 354,136-145.

[4] J.Smit&H.P.J.Wijn, (1959). "Ferrites" Physical Properties ofFerrimagneticOxides inrelation to their technical applications. Eindhoven: Phillips

[5] Maghsoudi I., Shokrollahi H., Hadianfard M.J. and Amighian J., (2013) Synthesis and characterization of NiAlxFe2–xO4 magnetic spinel ferrites produced byconventionalmethod Powder Technology, 235, 110–114.

[6] Mozaffari M. and Amighian J., (2003), Preparation of Alsubstituted Ni ferrite powders viamechanochemical processing *Journal of Magnetism and Magnetic Materials*, 260, 244–249.

[7] R. Sharma, S. Singhal, "Structural, magnetic andelectrical properties of zinc doped nickel ferrite andtheir application in photo catalytic degradation ofmethylene blue", *Physica B*, 414 (2013) 83–90